ARTICLE

Electrospun Nylon Nanofibers as Effective Reinforcement to Polyaniline Membranes

Angel Romo-Uribe,*,† Layza Arizmendi,‡ María Eugenia Romero-Guzmán,† Selene Sepúlveda-Guzmán,§ and Rodolfo Cruz-Silva||

Laboratorio de Nanopolímeros y Coloides, Instituto de Ciencias Físicas, Universidad Nacional Autónoma de México, Cuernavaca, Mor. 62210, México, Centro de Investigación en Ingeniería y Quimica Aplicada, Blvd. Enrique Reyna Hermosillo 140, Saltillo, Coahuila, México, Centro de Innovación, Investigación y Desarrollo en Ingeniería y Tecnología, Universidad Autónoma de Nuevo León, Monterrey, Nuevo León, México, and Centro de Investigación en Ingeniería y Ciencias Aplicadas, Universidad Autónoma del Estado de Morelos, Cuernavaca, Mor. 62210, México

ABSTRACT This research demonstrates that a nylon nanofiber (NNF) mat can be an effective mechanical reinforcement to polyaniline (PANI) thin films. Nanofibers of ca. 250 nm diameter were produced by electrospinning of a nylon 6 solution in formic acid. Scanning electron microscopy showed that the solution impregnation method utilized was effective to embed the nanofibers into the PANI matrix. The effectiveness of NNFs as a mechanical reinforcement of a PANI thin film was assessed via dynamic mechanical analysis in tension mode. The as-cast PANI films displayed a tensile dynamic modulus, E', of ca. 0.65 GPa at room temperature. Scanning in the temperature showed that the PANI film has a usage temperature of up to about 80 °C, with this being limited by its glass transition temperature, and over this temperature range, the elastic modulus was nearly independent of the temperature. On the other hand, the PANI−NNF composite displayed a significantly higher tensile modulus at room temperature (1.1 GPa) and its usage temperature was extended up to just over 200 °C, with this being limited by the melting transition of nylon 6 (at 220 °C). The results therefore showed that the NNF mat increased the usage temperature of PANI films over 100 °C, opening up applications for PANI membranes.

KEYWORDS: polyaniline • nanofiber • electrospinning • mechanical properties

INTRODUCTION

Polyaniline (PANI) is an intrinsically conductive polymer with many potential applications because of its low-cost synthesis, relatively easy processability, and environmental stability (1). This polymer is usually synthesized in an aqueous acidic solution, resulting in a dark-green electrically conductive powder. After treatment with ammonia, the polymer changes its color to dark blue and becomes nonconductive and solution-processable in organic solvents. *N*-Methylpyrrolidinone (NMP) is a very good solvent for PANI, and solutions up to 20 wt % can be prepared with the aid of low-molecular-weight additives (2−4). Free-standing PANI films or membranes can be obtained from these solutions by either evaporation or phase-inversion techniques. These films find interesting applications as actuators (5, 6), in nanofiltration processes (7), and in gas (8, 9) or liquid (10) separation systems. Indeed, since the first report of the potential of these films as highly selective membranes for gas separation (8), a great deal of work has been carried out in order to improve their performance. Some reports, however, address some drawbacks such as poor mechanical properties and their tendency to tear or puncture during operation. It is well-known that, during casting of PANI solutions in NMP, cross-linking occurs even at moderate temperatures and a fraction of the solvent remains in the film as a plasticizer (11, 12). The cross-linking affects the mechanical properties, resulting in brittleness and reducing the doping capability of the polymer, a process responsible for their separation selectivity. Several approaches have been employed to avoid these problems. Chemical cross-linking (13) was studied as an alternative to confer stability to these membranes without affecting the doping capability. In order to obtain a higher flux during separation, either an increase in the temperature or pressure of operation or a decrease in the membrane thickness is desirable. However, both of these processes can lead to a failure of the membrane by puncturing or tearing. These can be avoided either by reinforcing or by supporting the membrane on a net or mesh or another porous film. Metallic grids are commonly used to support separation membranes; for instance, stainless steel grids have been used to support an inorganic film for gas separation applications (14). On the other hand, for polymer films, reinforcement or a porous additional layer with better mechanical properties seems more feasible. Bilayer films using different polymer supports have been reported (9). Thin dense films of PANI have been supported in poly(vinylidene difluoride), as reported by Gupta et al. (15). Lee et al. (16) reported the use of bilayer membranes prepared by adhering a porous nylon membrane (0.2 μm pore size) to PANI cast films by using NMP. On the other hand, Spinks et al. (17) used carbon nanotubes to reinforce

* To whom correspondence should be addressed. E-mail: aromo-uribe@fis.unam.mx.

Received for review July 04, 2009 and accepted October 14, 2009

† Universidad Nacional Autónoma de México.

‡ Centro de Investigación en Ingeniería y Quimica Aplicada.

§ Universidad Autónoma de Nuevo León.

|| Universidad Autónoma del Estado de Morelos.

DOI: 10.1021/am900456a

Published on Web 10/26/2009

PANI films used as actuators. Besides porous membranes, electrospun nonwoven mats are ideal materials for membrane reinforcement. They possess not only a high porosity but also a completely interconnected pore structure, which allows high flux during separation. Contrary to metal nets, nonwoven mats are elastic, light-weight, chemically stable, and more compatible with the PANI because they can deform when the membrane is pressurized, avoiding the stress at the interface that might eventually lead to critical failure of the membrane. Electrospun polymer nanofibers are highly oriented and are being heavily studied as possible new reinforcing elements in polymer composites. Recently, electrospun cellulose fibers were mixed with polysuccinate to prepare a biodegradable composite (18). Nylon nanofibers (NNFs) have been successfully employed to reinforce dental composites (19, 20). Nylon, epoxy, and thermoplastic polyurethane nanofibers were used to reinforce laminated glass fiber−epoxy composites (21). Mather et al. have reported on the application of an ion-exchange membrane based on sulfonated poly(arylene ether sulfone) electrospun nanofibers (22). Thus, because of its adequate morphology and it being an interesting material, its application to reinforce membranes has just recently started.

In this work, we demonstrate that a thin electrospun nonwoven mat of NNFs can act simultaneously as a mechanical support and reinforcement layer for PANI membranes. The electrically conducting polymer surrounds each nanofiber, thus restricting fiber swelling due to moisture absorption, whereas the nanofiber mat provides mechanical strength to the membrane. Moreover, the interconnecting nanofiber structure ensures stress transfer through percolation pathways (i.e., there will be no stress concentration). The morphology, thermal transition, microstructure, and dynamic mechanical behavior are presented. The nanofiber mat effectively reinforced the film, increasing the usage temperature range in more than 100 °C and making these kinds of materials an attractive alternative to increase the performance of PANI films.

EXPERIMENTAL SECTION

Materials. Nylon 6 was a product from Nylon of Mexico, with a number-average molecular weight, without extractable, of 18 700 g/mol. Aniline was purchased from Aldrich, distilled at reduced pressure, and stored in the dark before use. Analytical-grade *N*-methylpyrrolidinone (NMP), ammonium persulfate, formic acid, hydrochloric acid, and ammonium hydroxide were purchased from Aldrich and used as received.

Nylon Nanofiber (NNF) Mat. Electrospinning of nylon 6 was carried out by a slight modification of the conditions reported by Ryu et al. (23). Nylon was dissolved in formic acid at a concentration of 20 wt % by gentle magnetic stirring overnight. Fiber electrospinning was carried out by applying a 0.2 mL/h flow rate, 15 kV potential, and 12 cm tip-to-target distance. The NNFs were collected on aluminum foil, and the resulting mat was cut and folded as a casting plate.

Preparation of PANI. PANI was synthesized by chemical oxidation of aniline using ammonium persulfate. First, aniline was dissolved in a 1.0 N hydrochloric acid solution to give a 0.3 M aniline solution.. This solution was cooled to −5 °C and degassed by bubbling nitrogen for about 30 min. Then a solution of ammonium persulfate in a 1.0 M hydrochloric acid solution was added dropwise. The oxidizer addition lasted 2 h, and the final concentration of both aniline and ammonium persulfate was 0.2 N. The reaction was carried under mild nitrogen bubbling, and the temperature was kept between −5 and −8 °C. These conditions usually yield PANI with a high weight-average molecular weight, $\bar{M}_w$, and fewer chain defects (24) compared to PANI synthesized at room temperature. After synthesis, PANI was filtered, and the filtered cake was then washed with distilled water. Then, the polymer was suspended in an excess of a 0.2 N ammonium hydroxide solution for 2 h, filtered, and washed with distilled water and finally with methanol. After drying at 40 °C, the dark-blue powder was stored in a desiccator.

Preparation of PANI and PANI−NNF Composite Membranes. In order to cast the PANI films, a 2 wt % solution of PANI in NMP was prepared by stirring the solution overnight at room temperature. The solution was centrifuged at 3400 rpm for 15 min, and the supernatant was poured onto either aluminum plates or the previously prepared NNF-coated aluminum plates and dried at 80 °C under a stream of air. The as-cast PANI films and PANI−NNF composite films were separated from the plates by soaking in distilled water.

Thermal Analysis. The thermal transitions were determined by differential scanning calorimetry (DSC). For DSC experiments, the Q200 calorimeter manufactured by TA Instruments (Newcastle, DE) was used. Temperature and enthalpy calibration were carried out using analytical-grade indium ($T_m = 156.6$ °C), and corrections were made for the instrument "baseline". The thermal transitions were determined at a heating rate of 20 °C/min. The decomposition temperatures, T_{dec}, were determined by thermogravimetric analysis (TGA), scanning at 20 °C/min, using the Q500 analyzer (manufactured by TA Instruments, Newcastle, DE). The thermal scans were carried out under a dry nitrogen atmosphere.

Dynamic Mechanical Analysis (DMA). DMA was performed using a Q800 dynamic mechanical analyzer (TA Instruments, Newcastle, DE). Dynamic frequency/temperature scans were carried out in tension mode over a temperature range from 0 to 220 °C; the heating rate used was 2 °C/min. Activation energy analysis requires the use of frequency scans at each temperature through the mechanical relaxation of interest.

Uniaxial Tensile Testing. Uniaxial tensile tests were carried out at room temperature using the TST-350 mini-tensile tester manufactured by Linkam Scientific Instruments Ltd. (Surrey, United Kingdom). Dog-bone-shaped samples were cut and tested using a strain rate of 5 mm/min.

X-ray Scattering. Two-dimensional patterns were obtained using a three-pinhole collimation S-Max3000 wide-angle X-ray scattering (WAXS)/small-angle X-ray scattering (SAXS) system manufactured by Rigaku. WAXS patterns were recorded using a flat-plate camera and Fuji image plates; a sample-to-detector distance of 6 cm was used, and the exposure time was set to 40 min. The patterns were analyzed using the X-ray scattering software POLAR v2.6 (Stonybrook Technology Inc., Stonybrook, NY).

Scanning Electron Microscopy (SEM). SEM was performed on a Hitachi S-4500II operating at 10 kV. The SEM cross-sectional images were acquired from fractured films under liquid nitrogen and coated with a thin gold layer. The diameter size distribution of the NNFs was obtained by analysis of the SEM images using CARNOY 2.0 image analysis software.

RESULTS AND DISCUSSION

Morphology and Microstructure. Electrospun techniques have been previously studied, and the effect of parameters such as the voltage, tip-to-target distance, and polymer concentration on the morphology of the resulting fibers has been elucidated (25, 26). In this work, nylon fibers

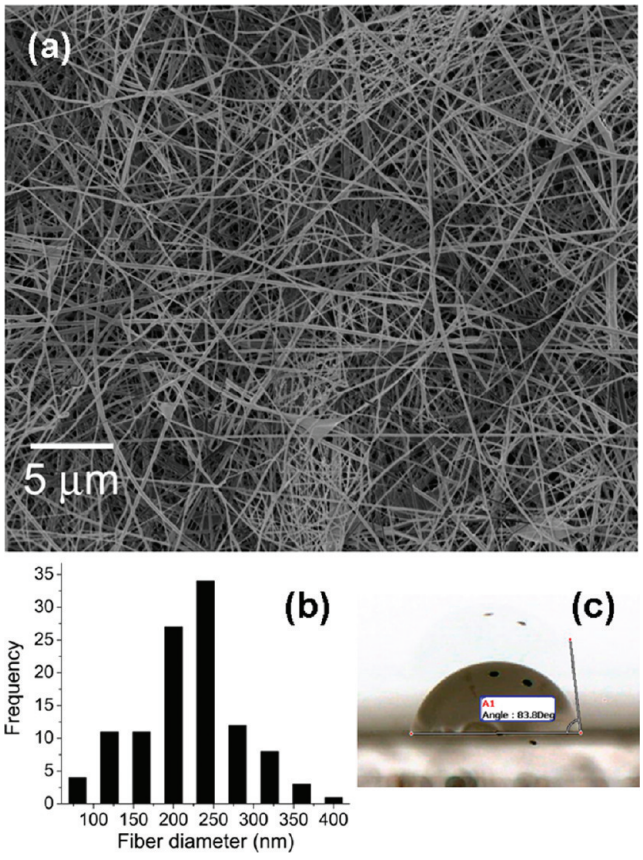

FIGURE 1. (a) SEM micrograph of electrospun NNFs. (b) Distribution of fiber diameters. (c) Contact-angle image of water on the NNF mat (the angle is 83.8°).

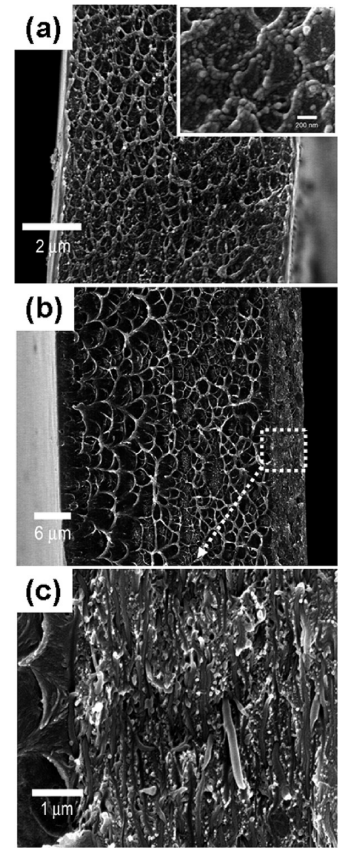

FIGURE 2. SEM micrographs of (a) an as-cast PANI film (the inset shows the cross section at higher magnification), (b) a PANI−NNF composite, and (c) a PANI−NNF composite at higher magnification.

were prepared by using a standard method previously reported, and Figure 1 shows the SEM image of the as-spun mat.

It can be seen that the fibers have a smooth surface, random orientation, and broad diameter distribution. Image analysis showed that the number-average diameter was 250 nm (the fiber diameter distribution ranged from 90 to 400 nm, as shown by the histogram in Figure 1b). No evidence of defects such as beads or ribbons was found. In order to obtain a thick mat, the fibers were collected for several minutes until a highly porous mat of fibers of about 6 μm thickness was obtained. A reinforced PANI film was prepared by casting a PANI−NMP solution onto the NNF mat. PANI was infiltrated into the void of the NNF mat by capillarity aided by the high porosity and hydrophobic properties of the nylon mat (see Figure 1c).

Figure 2 shows the SEM images of the cross section of fractured PANI and NNF-reinforced PANI films. The fractured surface of the PANI film (Figure 2a) reveals a dense film with morphology that arises from the casting process. PANI solutions in NMP contain a large fraction of small polymer aggregates (15−30 nm) that are swollen with the solvent. After drying, these aggregates can still be seen at high magnification (Figure 2a, inset).

The SEM image of the composite PANI−NNF film shows an asymmetrically reinforced membrane (Figure 2b). A dense PANI layer combined with a 6-μm-thick PANI−NNF layer can be clearly seen. Figure 2c shows that there is an intimate contact between the matrix and the nanofibers because the matrix is surrounding the nanofibers and completely filling the interfiber voids. The good adhesion shown at the interface might be the result of the hydrogen bonding between the amine and the carbonyl moieties of PANI and the nylon, respectively (27).

The microstructures of the PANI film and the PANI−NNF membrane were also investigated by WAXS. Figure 3a shows the WAXS pattern of an as-cast PANI film. The pattern shows an intense amorphous halo with uniform intensity around the azimuth. The halo is the signature of an amorphous (glassy) polymer. On the other hand, the uniform intensity around the azimuth indicates the absence of any preferred molecular orientation. Figure 3b shows the corresponding azimuthally averaged radial intensity trace; the intensity maximum is located at $2\theta = 19.2°$, corresponding to a mean correlation length of 4.6 Å.

On the other hand, the WAXS pattern of the PANI−NNF membrane shows a narrower (in 2θ) amorphous halo and an outer (weak) crystalline reflection arising from the nylon component (Figure 3c). It is noted that the halo shows a constant intensity around the azimuth, indicating that the nanofibers in the membrane are randomly oriented. Figure 3d shows the corresponding azimuthally averaged intensity trace, where the intensity trace of nylon 6 (labeled N6, bottom trace) has been added for the sake of reflection identification. The strongest crystalline reflections of nylon

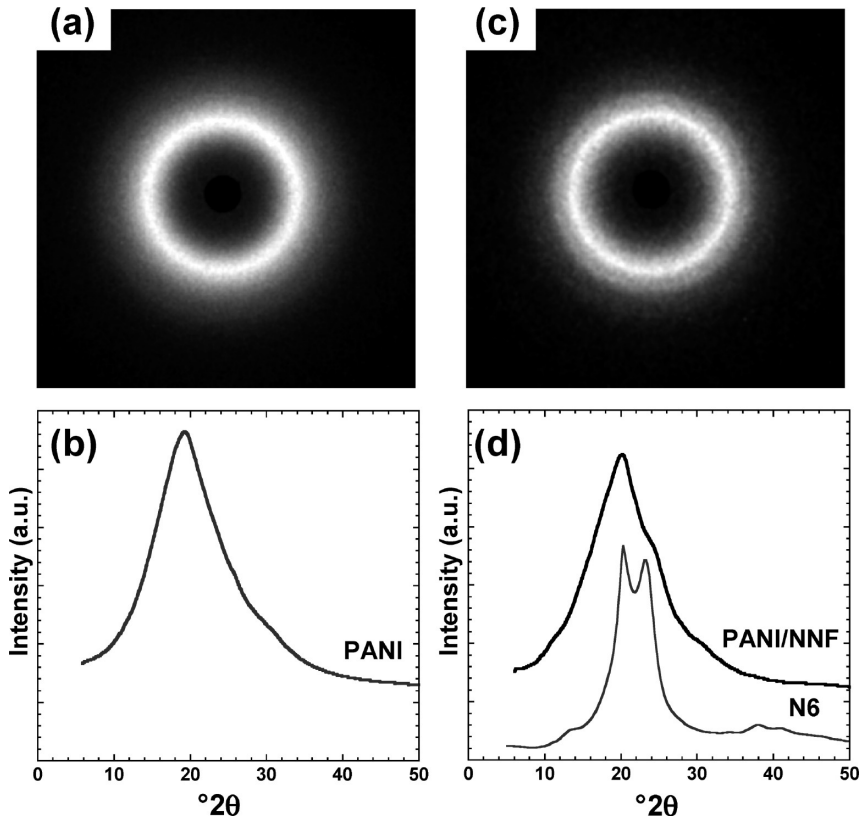

FIGURE 3. WAXS patterns and azimuthally averaged intensity profiles of (a and b) as-cast PANI films and (c and d) PANI−NNF composite films.

6 are located at $2\theta = 20.3°$ and 23.3°, corresponding to d spacings of 4.4 and 3.8 Å. Whereas the $2\theta = 20.3°$ reflection is washed out by the stronger amorphous halo of PANI, the $2\theta = 23.3°$ reflection is clearly seen as a shoulder on the PANI−NNF intensity trace. The poor crystallinity exhibited by the PANI−NNF composite suggests a quenching process during solvent evaporation in the electrospinning process, thus preventing further crystallization of the NNFs, in agreement with previous reports (28).

Thermal Properties. Figure 4a shows the TGA scans of (i) an as-cast PANI film and (ii) the PANI−NNF membrane. The PANI film shows monotonic weight loss up to about 100 °C, where the trace reaches a plateau and the film has lost 5% of its original weight. The initial weight loss is usually residual water, absorbed during the immersion process carried out to separate the films from the casting plate. As the temperature is increasing, the weight remains constant up to about 170 °C, where there is an onset of weight loss; by 230 °C, the film has lost 10% of its original weight. These weight losses correspond to residual NMP, which has a boiling point close to 200 °C. A further increase of the temperature produces a weight loss at a constant rate until the onset of degradation is reached at ca. 441 °C and the material rapidly loses about 60% of the original weight. The weight loss onsets are clearly seen as maxima in the corresponding weight derivative trace shown in Figure 4b. The activation energy for thermal degradation, $E_{a,dec}$, was determined using Broido's equation (29), and the resulting values are summarized in Table 1.

The TGA trace of the PANI−NNF membrane shows weight loss onsets similar to that of the PANI film. However, the weight loss is significantly attenuated for the membrane (for instance, at 230 °C, PANI−NNF has only lost about 5% weight vs 10% of PANI). However, the results show that the nanofiber mat dominates degradation of the membrane. The onset for degradation occurs at 396 °C, which corresponds to degradation of nylon 6 (see Table 1). Note that at ca. 440 °C there is a change of the weight loss rate due to the presence of PANI (the weight derivative shows two maxima, clearly identifying the weight loss onset of the two phase-separated components). Note that the activation energy for degradation was found to be significantly higher for the membrane (see Table 1).

The thermal transitions were characterized by DSC; the DSC traces corresponding to the first and second heating scans are shown in Figure 5a,b, respectively. The as-cast PANI film (trace i) showed a glass transition temperature, T_g, of 208 °C from the first heating scan. The second heating scan showed an increase in T_g, estimated in this case at about 218 °C. The increase in the glass transition temperature after the first heating scan was consistent with the elimination of NMP (detected by TGA; Figure 4, trace i), which acts as a plasticizer (4).

On the other hand, the first heating scan of the PANI−NNF membrane (Figure 5a, trace ii) shows a broad endothermic peak at about 100 °C. This endotherm is associated with water trapped in PANI as a result of the immersion process carried out to separate the films from the casting plate. A

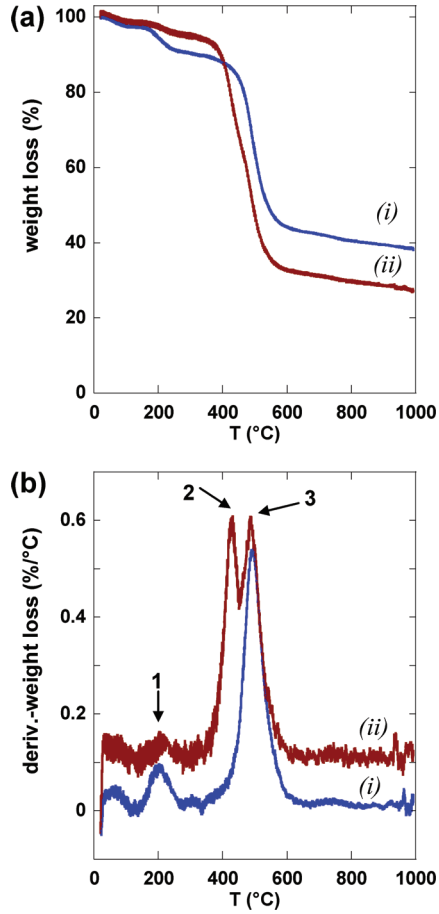

FIGURE 4. (a) Weight loss as a function of the temperature as determined by TGA. (b) Weight loss derivative traces. TGA traces correspond to (i) PANI and (ii) PANI−NNF composite films.

second (and weaker) endothermic peak was found at 218 °C, due to the nylon melting transition. The second heating scan (Figure 5b, trace ii) shows only the endothermic peak associated with the solid-to-melt transition of nylon because water had been evaporated during the first heating scan. In this case, there is no evidence of the glass transition of PANI, probably because of overlap with the broad endothermic peak. DSC does not have enough resolution to detect this transition, although it is known that in a phase-separated composite the thermal transitions are differentiated for each component. The DMA results will show the individual thermal transitions and mechanical relaxations of the membrane components because this technique is much more sensitive to thermal transitions than DSC.

DMA Properties. The mechanical properties of the as-cast PANI film and the composite PANI−NNF were characterized by using DMA in tension mode. Furthermore, temperature/frequency scans were carried out in order to characterize mechanical relaxations and determine their activation energies. Strain sweeps, at a constant frequency of 1 Hz, were carried out in order to determine the linear viscoelastic (LVE) regime of each specimen. The results showed that PANI and PANI−NNF displayed a LVE regime from strain as low as 0.5% and up to about 1.4%. Thus, the temperature/frequency scans were carried out at a constant strain of 0.8% and a heating rate of 2 °C/min, and the frequency was varied from 0.5 to 50 Hz. Figure 6 shows a plot of dynamic tensile modulus E' as a function of the temperature, at 1 Hz. The upper temperature limit in this plot was defined by the failure of each specimen. This temperature is lower than that reported for PANI films before (4), but the difference can be ascribed to the differences in thickness (70 vs 25 μm in this work). Trace a corresponds to the storage modulus of the PANI film. The modulus behaved nearly independently of the temperature, with a value of 0.7 GPa. The temperature scan showed a small inflection at about 50 °C, and the modulus was reduced to ca. 0.62 GPa, soon after the film tore apart.

On the other hand, the PANI−NNF composite film showed initially a storage modulus of ca. 1.1 GPa, significantly higher than that of the PANI film. The reinforcing effect of the NNF mat was confirmed by uniaxial tensile testing. The results showed that for the PANI film the Young modulus $Y = 0.92$ GPa with an elongation at break of 3.2%, whereas for the PANI−NNF composite $Y = 1.2$ GPa with an elongation at break of 3.0%.

Regarding the DMA results, the dynamic mechanical modulus of the PANI−NNF film showed two mechanical relaxations; at about 90 °C, the modulus decayed to 0.77 GPa, and then at about 160 °C, the modulus decayed to 0.65 GPa and remained constant before the composite failed at a temperature just over 200 °C, some 20 °C below the melting transition temperature of nylon 6. Thus, the composite showed a significant increase in the working temperature range of over 100 °C with respect to the neat PANI film. We ascribe this improvement in the performance to the nanofiber mat of nylon. PANI films usually become brittle at high temperature, and under cyclic load, the failure might involve crack propagation. However, the NNFs are most likely working as an effective reinforcement, avoiding crack propagation. In this sense, the PANI−NNF composite might behave similarly to long-glass fiber-reinforced composites.

The reductions in the storage modulus are associated with mechanical relaxation associated with the molecular and local motion of the molecular chains. The mechanical relaxations are easily identified as maxima from the plots of mechanical damping tan δ as a function of the temperature, shown in Figure 7. Figure 7a shows the plot of tan δ as a function of the temperature for the as-cast PANI film at the frequencies (i) 0.5, (ii) 10, and (iii) 50 Hz. There are two transitions identified at 50 Hz (trace iii), where a first maximum appears at 33 °C and then a second maximum occurs at 66 °C. These mechanical relaxations are tentatively denoted as the γ and β transitions, respectively. Note that the α transition, associated with the glass transition, cannot be attained in the tension mode utilized here because of the failure of the PANI film before reaching the glass transition. Thus, these lower temperature transitions would be associated with local, short-range, molecular motions. A further investigation is being carried out in order to elucidate the nature of those relaxations.

On the other hand, Figure 7b shows the plot of tan δ as a function of the temperature for the PANI−NNF composite

Table 1. Thermal Properties of PANI, Nylon 6, and a PANI−NNF Composite[a]

			T_g (°C)		T_m (°C)	
sample	$T_{dec,onset}$ (°C)	$E_{a,dec}$[b] (kJ/mol)	first heat	second heat	first heat	second heat
PANI	441	9.2	208	218		
nylon	401					220
PANI−NNF	396	16.5			218	217
	440					

[a] T_{dec} = decomposition temperature, $E_{a,dec}$ = activation energy for decomposition, T_g = glass transition temperature, and T_m = melting temperature. [b] From Broido's equation (29).

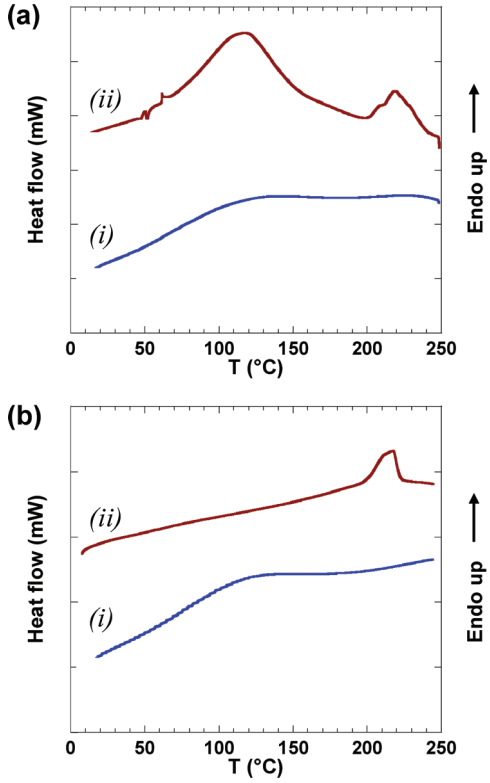

FIGURE 5. DSC scans for the (a) first and (b) second heatings, (i) an as-cast PANI film, and (ii) PANI−NNF composites.

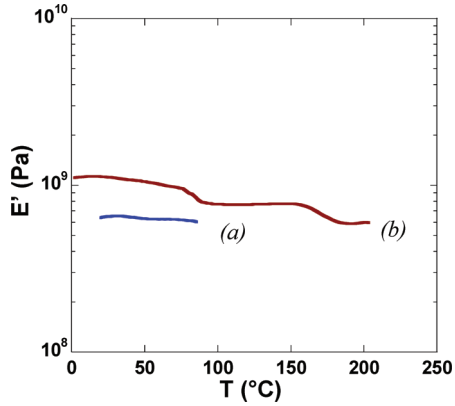

FIGURE 6. Elastic shear modulus (E') as a function of the temperature at 1 Hz frequency for (a) an as-cast PANI film and (b) a PANI−NNF composite.

at the frequencies (iv) 0.5, (v) 5, and (vi) 50 Hz. There are in this case three maxima in tan δ, at 180, 80, and 40 °C; these relaxations are termed α, β, and γ, respectively. The transition marked as β at 80 °C appears to be associated with the α transition of nylon 6 (see Table 2). The transition termed

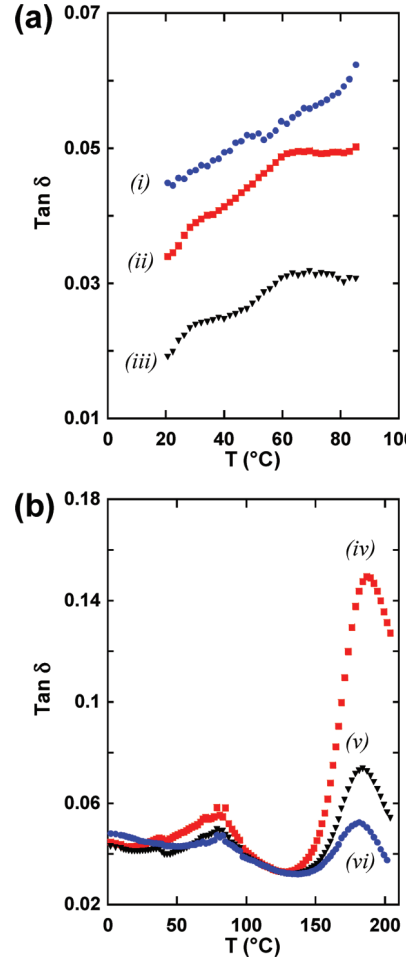

FIGURE 7. Mechanical damping tan δ as a function of the frequency of oscillation and temperature for (a) an as-cast PANI film at (i) 0.5, (ii) 10, and (iii) 50 Hz and (b) a PANI−NNF composite film at (iv) 0.5, (v) 5, and (vi) 50 Hz.

Table 2. DMA Properties of PANI, Nylon 6, and a PANI−NNF Composite

sample	T_γ (°C)	$E_{a,\gamma}$ (J/mol)	T_β (°C)	$E_{a,\beta}$ (J/mol)	T_α (°C)	$E_{a,\alpha}$ (J/mol)
PANI	33	558	66	299		
nylon 6			−44		76	630
PANI−NNF	40		80		180	1300

α at 180 °C is suggested to originate from the interaction between PANI and the NNF mat. We arrived at this suggestion because a DMA temperature scan carried out on a neat nylon 6 film, up to its melting temperature of 225 °C, did not show any mechanical relaxation above 80 °C. On the other hand, the DSC results showed that the glass transition

of the PANI film occurs around 208 °C. Thus, the transition at 180 °C appears to be associated with the composite rather than the individual components. Moreover, note that the 180 °C relaxation is much more intense than the lower temperature relaxations and the mechanical damping also increases at lower frequencies. It is suggested that this transition is associated with the interaction of PANI and NNF. That is, at lower frequencies (longer relaxation times), the interaction between PANI and nanofibers is more enhanced, thus dissipating more energy (i.e., larger tan δ peak). On the other hand, at high frequencies (shorter relaxation times), local molecular vibrations are favored and the interaction between PANI and nanofibers is reduced, lowering therefore the energy dissipation (i.e., smaller tan δ peak).

There are indeed more aspects to be investigated regarding the microstructure and thermal annealing effects on the NNFs (influence of the degree of crystallinity, degree of molecular orientation, and nanofiber diameter among others) and the composite. However, the results of this investigation suggest that the nanofiber network membrane displays a more desirable morphology and better mechanical properties than, say, a metal grid membrane as far as reinforcing the PANI thin films is concerned.

CONCLUSIONS

Polymer-impregnated nonwoven mats have been used as structural composites for many years ago. However, in this work, we demonstrated that this approach can also be applied in the nanoscale to prepare NNF-reinforced PANI thin films. The working temperature of the resulting PANI—NNF films was increased by more than 100 °C, which might be a great improvement for gas separation technologies. Good interfacial adhesion between the polymers is suggested by the SEM images and the DMA studies. The upper working temperature of the composite was defined by the melting transition of NNFs. The method shown here is very simple yet efficient and can be extended to different polymers. Further research on the reinforcement and failure mechanism is being carried out.

Acknowledgment. The support of Prof. Patrick T. Mather (Syracuse University) is gratefully acknowledged. M.E.R.-G. was supported by a postdoctoral fellowship from DGAPA-UNAM. The authors also thank the anonymous reviewers; the manuscript has benefited from their insightful comments. This research was partially supported by CONACyT (CIAM-2006, Project 58646) and PROMEP (NPTC-151).

REFERENCES AND NOTES

(1) MacDiarmid, A. G. *Appl. Phys.* **2001**, *1*, 269–279.
(2) Zheng, W.; Angelopoulos, M.; Epstein, A. J.; MacDiarmid, A. G. *Macromolecules* **1997**, *30*, 7634–7637.
(3) Yang, D.; Lu, W.; Goering, R.; Mattes, B. R. *Synth. Met.* **2008**, *159*, 666–674.
(4) Wei, Y.; Jang, G.-W.; Hsueh, K. F.; Scherr, E. M.; MacDiarmid, A. G.; Epstein, A. J. *Polymer* **1992**, *33*, 314–322.
(5) Smela, E. *MRS Bull.* **2008**, *33*, 197–204.
(6) Gao, J. B.; Sansiñena, J. M.; Wang, H. L. *Chem. Mater.* **2003**, *15*, 2411–2418.
(7) Gloukhovski, R.; Oren, Y.; Linder, C.; Freger, V. *J. Appl. Electrochem.* **2008**, *38*, 759–766.
(8) Anderson, M. R.; Mattes, B. R.; Reiss, H.; Kaner, R. B. *Science* **1991**, *252*, 1412–1415.
(9) Illing, G.; Hellgardt, K.; Wakemana, R. J.; Jungbauer, A. *J. Membr. Sci.* **2001**, *184*, 69–78.
(10) Huang, S. C.; Ball, I. J.; Kaner, R. B. *Macromolecules* **1998**, *31*, 5456–5464.
(11) Tan, H. H.; Neoh, K. G.; Liu, F. T.; Kocherginsky, N.; Kang, E. T. *J. Appl. Polym. Sci.* **2001**, *80*, 1–9.
(12) Mathew, R.; Yang, D.; Mattes, B. R.; Espe, M. P. *Macromolecules* **2002**, *35*, 7575–7581.
(13) Loh, X. X.; Sairam, M.; Bismarck, A.; Steinke, J. H. G.; Livingston, A. G.; Li, K. *J. Membr. Sci.* **2009**, *326*, 635–642.
(14) Yin, X.; Zhu, G. S.; Yang, W.; Li, Y.; Zhu, G. Q.; Xu, R.; Sun, J.; Qiu, S.; Xu, R. R. *Adv. Mater.* **2005**, *17*, 2006–2010.
(15) Gupta, Y.; Hellgardt, K.; Wakeman, R. J. *J. Membr. Sci.* **2006**, *282*, 60–70.
(16) Lee, Y. M.; Ha, S. Y.; Lee, Y. K.; Suh, D. H.; Hong, S. Y. *Ind. Eng. Chem. Res.* **1999**, *38*, 1917–1924.
(17) Spinks, G. M.; Xi, B.; Truong, V.-T.; Wallace, G. G. *Synth. Met.* **2005**, *151*, 85–91.
(18) Han, S. O.; Son, W. K.; Youk, J. H.; Park, W. H. *J. Appl. Polym. Sci.* **2008**, *107*, 1954–1959.
(19) Tian, M.; Gao, Y.; Liu, Y.; Liao, Y.; Xu, R.; Hedin, N. E.; Fong, H. *Polymer* **2007**, *48*, 2720–2728.
(20) Lin, S.; Cai, Q.; Ji, J.; Sui, G.; Yu, Y.; Yang, X.; Ma, Q.; Wei, Y.; Deng, X. *Compos. Sci. Technol.* **2008**, *68*, 3322–3329.
(21) Liu, L.; Huang, Z.-M.; He, C. L.; Han, X. J. *Mater. Sci. Eng. A* **2006**, *435—436*, 309–317.
(22) Choi, J.; Lee, K. M.; Wycisk, R.; Pintauro, P. N.; Mather, P. *Macromolecules* **2008**, *41*, 4569–4572.
(23) Ryu, Y. J.; Kim, H. Y.; Lee, K. H.; Park, H. C.; Lee, D. R. *Eur. Polym. J.* **2003**, *39*, 1883–1889.
(24) Adams, P. N.; Laughlin, P. J.; Monkman, A. P.; Kenwright, A. M. *Polymer* **1996**, *37*, 3411–3417.
(25) Zhang, C.; Yuan, X.; Wu, L.; Han, Y.; Sheng, J. *Eur. Polym. J.* **2005**, *41*, 423–432.
(26) Zhang, S.; Shim, W. S.; Kim, J. *Mater. Des.* **2009**, *30*, 3659–3666.
(27) Sung, W. B.; Seung, S. I. *Polymer* **1998**, *39*, 485–489.
(28) Stephens, J. S.; Chase, D. B.; Rabolt, J. F. *Macromolecules* **2004**, *37*, 877–881.
(29) Broido, A. *J. Polym. Sci., Polym. Phys. Ed.* **1969**, *7*, 1761–1773.

AM900456A